X-ray evidence of a native state with increased compactness populated by tryptophan-less *B. licheniformis* β-lactamase

Valeria A. Risso,[1,2] Juan P. Acierno,[1,2] Stefano Capaldi,[3] Hugo L. Monaco,[3] and Mario R. Ermácora[1,2]*

[1]Departamento de Ciencia y Tecnología, Universidad Nacional de Quilmes, Roque Sáenz Peña 325, (1876) Bernal, Buenos Aires, Argentina

[2]Instituto Multidisciplinario de Biología Celular, Conicet-Cicpba, Calle 526 y Camino Gral. Belgrano, (B1906APO) La Plata, Buenos Aires, Argentina

[3]Biocrystallography Laboratory, Department of Biotechnology, University of Verona, Ca Vignal 1, Strada Le Grazie 15, Verona, Italy

Received 26 January 2012; Revised 25 March 2012; Accepted 29 March 2012
DOI: 10.1002/pro.2076
Published online 11 April 2012 proteinscience.org

Abstract: β-lactamases confer antibiotic resistance, one of the most serious world-wide health problems, and are an excellent theoretical and experimental model in the study of protein structure, dynamics and evolution. *Bacillus licheniformis* exo-small penicillinase (ESP) is a Class-A β-lactamase with three tryptophan residues located in the protein core. Here, we report the 1.7-Å resolution X-ray structure, catalytic parameters, and thermodynamic stability of $ESP^{\Delta W}$, an engineered mutant of ESP in which phenylalanine replaces the wild-type tryptophan residues. The structure revealed no qualitative conformational changes compared with thirteen previously reported structures of *B. licheniformis* β-lactamases (RMSD = 0.4–1.2 Å). However, a closer scrutiny showed that the mutations result in an overall more compact structure, with most atoms shifted toward the geometric center of the molecule. Thus, $ESP^{\Delta W}$ has a significantly smaller radius of gyration (R_g) than the other *B. licheniformis* β-lactamases characterized so far. Indeed, $ESP^{\Delta W}$ has the smallest R_g among 126 Class-A β-lactamases in the Protein Data Bank (PDB). Other measures of compactness, like the number of atoms in fixed volumes and the number and average of noncovalent distances, confirmed the effect. $ESP^{\Delta W}$ proves that the compactness of the native state can be enhanced by protein engineering and establishes a new lower limit to the compactness of the Class-A β-lactamase fold. As the condensation achieved by the native state is a paramount notion in protein folding, this result may contribute to a better understanding of how the sequence determines the conformational variability and thermodynamic stability of a given fold.

Keywords: protein compactness; protein folding; radius of gyration; protein packing; *B. licheniformis*; protein engineering; site-specific mutagenesis; β-lactam; penicillinase

---

Abbreviations: ESP, *Bacillus licheniformis* exo-small penicillinase; $ESP^{\Delta W}$ tryptophan-less ESP.

Additional Supporting Information may be found in the online version of this article.

Valeria A. Risso and Juan P. Acierno contributed equally to this work.

Grant sponsors: CONICET, UNQ, ANPCyT, LNLS (Brazil).

*Correspondence to: Mario R. Ermácora, Departamento de Ciencia y Tecnología, Universidad Nacional de Quilmes, Roque Sáenz Peña 325, (1876), Bernal, Buenos Aires, Argentina. E-mail: ermacora@unq.edu.ar

Introduction

Class-A β-lactamases attract large attention because they cause one of the most common bacterial resistances to antibiotics and have become a serious contemporary health problem. These enzymes hydrolyze β-lactam antibiotics and inactivate them as inhibitors of the bacterial cell-wall synthesis. The catalytic mechanism of Class-A β-lactamases has been thoroughly investigated,[1–5] and high-resolution X-ray structures and biochemical evidence have shown that it involves the transient acylation of a serine residue at the active site.

Besides its medical, microbiological, and pharmaceutical importance, Class-A β-lactamases have been paradigms in protein structure, dynamics, function, and evolution studies. For protein folding, these ~29 kDa proteins constitute a valuable experimental model that started to be studied very early. For instance, they were among the first well-characterized examples of proteins that populate partially folded states, and for that reason they became instrumental in the characterization of the molten globule state.[6–9]

Class-A β-lactamases have two domains. One, all-α-helical, is built with the middle part of the sequence. The other, an α + β domain, contains a five-stranded β-sheet comprising the N- and C-termini. This complexity raises questions of general relevance for multidomain proteins. For instance, do the domains fold asynchronously or concomitantly? If the first is true, is the all-α, continuous domain the template onto which the α + β domain folds, or is it the latter, discontinuous domain which surmounts a colossal entropic barrier and drives the folding of the former? Alternatively, if the protein folds after a general collapse with the two domains arising at the same time, what drives the backbone to an initial global arrangement compatible with such a large and complex final structure? These are only a few of the yet unanswered questions that continue to inspire a large amount of experimental and theoretical work and explain the enduring interest in the structure of Class-A lactamases.

Bacillus licheniformis exo-small penicillinase, ESP, is particularly well-suited for studying the folding of Class-A β-lactamases because it lacks disulfides, is thermodynamically very stable, populates several partially folded states under denaturing conditions, and has a fully reversible thermal transition.[10–15]

Wild-type ESP possesses three tryptophan residues that are utilized as intrinsic fluorescent probes to monitor the protein conformational transitions. However, despite an apparently favorable location of these three tryptophans in the protein matrix, their spectroscopic signals are not well resolved and not very informative of local conformational fluctuations. For that reason, we prepared and characterized the corresponding single-tryptophan and the tryptophan-free ESP variants.[16] Using these variants, in which tryptophan residues have been replaced by phenylalanine, the contributions of the individual tryptophans to the overall spectroscopic signals were characterized. Based on that characterization, it was concluded that the tryptophan-less variant, $ESP^{\Delta W}$, provides an optimized platform to engineer singly intrinsic fluorescence probes for monitoring specific domains and subdomains fluctuations during folding experiments.[16]

Very soon, however, we learned that these engineered variants had interesting structural and folding properties of their own. $ESP^{\Delta W}$ was particularly intriguing because it seemed to tolerate, with only a small loss of stability, the significant voids created by the mutations in the protein core. Moreover, the simplified spectroscopic signals from the remaining aromatic residues gave a hint of a subtle conformational adjustment.[16] With these considerations in mind, we undertook the characterization of $ESP^{\Delta W}$ using X-ray crystallography.

Here we will show that the subtle adjustment in the structure of $ESP^{\Delta W}$ illustrates a previously unrecognized response to mutations that create voids in the protein core. Commonly, point mutations cause modest and localized changes in the structure, and redesign of the core to maintain steric side chain complementariness is infrequent.[17–21] In the case of $ESP^{\Delta W}$, the void and lack of optimal complementariness between side chains are alleviated by a global movement of almost all the backbone atoms toward the geometric center of the molecule, resulting in a significantly increased compactness.

Packing density is a seminal concept in the study of protein structure, dynamic and evolution.[22,23] The case of $ESP^{\Delta W}$ shows that the compactness of the native state can be increased by protein engineering. It also suggests that the extant structures might have not evolved to optimize packing but rather to maintain a balance between this and other properties, such as flexibility and stability. Further, it suggests that a systematic analysis of packing density in X-ray structures using simple tools such as R_g calculations and statistical analysis of noncovalent distances may provide new insights on protein structure and folding.

Results

Crystallization, data collection, structure solution, and refinement

In the presence of 28% PEG 4000, at pH = 5.4 and 19°C, $ESP^{\Delta W}$ crystallizes after two weeks as flattened spindles of about 150 × 50 × 50 μm. The diffraction data could be integrated and scaled assuming that the crystals were orthorhombic and a

solution with reasonable packing was found by molecular replacement in space group $P2_12_12$. However, the R_{free} of this solution could not be lowered below 35%, which led to the conclusion that the correct space group had to be monoclinic with a β angle very close to 90°. In general, the nonright angle of biomacromolecular monoclinic crystals tends to differ significantly from 90° but in about 4% of the total population this angle is close enough to 90° to generate a pseudo orthogonal lattice. This was found to be the case of the $ESP^{\Delta W}$ crystals. The structure was solved by molecular replacement in the monoclinic space group $P2_1$ to a resolution of 1.73 Å (Table I). Two protein molecules are present in the asymmetric unit and they were treated independently during refinement. As the crystallization solution contained sodium citrate, the residual electron density present at the active site was modelled as a bound citrate anion. In the refined structure, chain A superimposed on chain B gave a RMSD = 0.16 Å. Coordinates and structure factors have been deposited in the PDB (ID: 3SOI).

Global fold and tertiary structure

$ESP^{\Delta W}$ adopts the characteristic Class-A β-lactamase fold, which features 12 main helical segments and one five–stranded antiparallel β-sheet grouped in two domains: the α domain comprising the sequentially central residues 66–212, and the α + β domain, comprising N- and C-terminal residues 29–60 and 220–291, respectively. The domains are built in such a way that the main chain connects them twice (residues 61–65 and 213–219). The catalytic pocket is located between the two domains.

The solved structure is very similar to the thirteen previously reported structures of *B. licheniformis* β-lactamases (RMSD = 0.4–1.2 Å; see Table II). There is only a minor backbone conformational change involving residues 102 and 103 that results in a significant increment of the static solvent accessible surface area of the Val 103 side chain (from 10 to 30%). This change is in a long loop that is quite far from the mutation sites but close to the active site, and therefore it might have an impact on the catalytic properties of $ESP^{\Delta W}$ (see below).

Local effects of the mutations

Replacing Trp by Phe at position 210 causes very little local perturbation (Fig. 1, panel A). The phenyl group occupies the place of the tryptophan pyrrole ring, and the void left by the three carbon atoms eliminated is compensated by a subtle inward shift of almost every atom close to the mutation and by a rotamer change affecting Leu 206. The most prominent structural change caused by the mutation of residue 210 is the unavoidable loss of a hydrogen bond between the Trp NE1 and the side chain carboxylate of Asp 124. Interestingly, a conserved water molecule that is at hydrogen–bond distance of the above nitrogen is also present in one of the chains of the mutant.

The solvent accessibility of residue 210 and the surrounding atoms is not affected by the mutation. Indeed, the solvent accessible surface of Trp 210 is less than 1% in the wild-type protein, and that of

Table I. *Data Collection, Refinement Statistic, and Quality of the Model*

A. Data collection	
Wavelength (Å)	1.43
Temperature (K)	100
Frames/total oscillation (°)	360/180
Space group	$P2_1$
Unit-cell parameters (Å, °)	$a = 42.76$
	$b = 110.09$
	$c = 54.13$
	$\alpha = 90.00$
	$\beta = 89.97$
	$\gamma = 90.00$
Resolution[a] (Å)	55.04–1.73 (1.82–1.73)
R_{merge}[b] (%)	6 (18.6)
$\langle I\rangle/\langle\sigma_{(I)}\rangle$	13.9 (5.7)
Completeness (%)	96.4 (93.5)
Total reflections	183797
Unique reflections	50182
Multiplicity	3.7 (3.5)
Average mosaicity (°)	0.626
Wilson B factor ($Å^2$)	11.82
Matthews coeff. ($Å^3$/Da)	2.22
Solvent fraction (%)	44.71
Number of copies/ASU	2
B. Refinement statistics	
Resolution (Å)	30.0–1.73 (1.77–1.73)
Total number of reflections	48,058
Working set: number of reflections	
R_{work}[c] (%)	17.1 (24.6)
Test set: number of reflections	
R_{free}[d] (%)	19.3 (27.2)
Nonhydrogen atoms	4328
Protein	3988
Ligand	26
Water	314
C. Geometry statistics	
Average isotropic B factors ($Å^2$)	
Protein atoms	8.0
Ligands	21.9
Water molecules	13.5
R.M.S. deviations	
Bond length (Å)	0.005
Bond angles (°)	1.360
Ramachandran plot[e]	
Most favoured (%)	89.8
Additionally allowed (%)	9.8
Generously allowed (%)	0.4
Outliers (%)	0

[a] Values in parentheses are for the highest resolution shell.
[b] $R_{merge} = \sum_{hkl}\sum_i |I_{hkl,i} - \langle I_{hkl}\rangle| / \sum_{hkl}\sum_i I_{hkl,i}$.
[c] $R_{work} = \sum |F_{obs} - F_{calc}| / \sum |F_{obs}|$, where F_{calc} and F_{obs} are the calculated and observed structure factor amplitudes, respectively.
[d] R_{free} is the same as R_{work}, but for 5.0% of the total reflections, chosen at random and omitted during refinement.
[e] As defined by PROCHECK.

Table II. *High-Resolution Structures of B. licheniformis β-Lactamases Included in the Study*

PDB ID	Strain	Mutation	Resolution (Å)	pH[a]	Temperature (K)	RMSD[b]	R_g[c]
3SOI[d]	749/C[e]	ΔW	1.7	5.4	100	0.00, 0.16	16.77
4BLM	749/C	—	2.0	5.5	n.a.	0.50, 0.50	17.13
1MBL	749/C	—	2.0	6.2	n.a.	0.58, 0.61	17.24
3LY3	749/C	E166C	1.8	7.5	n.a.	0.89	17.11
3LY4	749/C	E166C	1.8	7.5	n.a.	0.77	17.04
3SH7	749/C	E166C	2.5	7.5	291	0.97	17.15
3SH9	749/C	E166C	1.9	7.5	n.a.	1.15	17.15
3M2J	749/C	E166C	1.8	7.2	100	0.53, 0.50	17.09
1I2S	BS3[f]	—	1.9	5.0	288	0.47, 0.49	17.07
1I2W	BS3	—	1.7	5.0	288	0.50, 0.51	17.10
1W7F	BS3	—	1.8	n.a.	100	0.49, 0.51	17.05
2X71	BS3	—	2.1	4.0	100	0.42, 0.40	16.93
2WK0	BS3	—	1.6	3.4	293	0.48, 0.49	17.06
3B3X	BS3	—	2.5	7.2	100	0.57, 0.54	17.05

[a] Crystallization pH.
[b] Backbone superposition to chain A in soi3.pdb. The second value indicates the RMSD for chain B, when present in the asymmetric unit.
[c] The radius of gyration was calculated for 1020 structurally equivalent backbone atoms.
[d] The structure of $ESP^{\Delta W}$ reported in this work.
[e] Sequence UNP ID: 4 P00808.
[f] Sequence UNP ID: P94458 (the sequence differences with P00808 are: A59T, A133T, V187A, R191A, D227E, A238G, L287M).

Phe 210 in the mutant is nearly the same. Interestingly, the packing of atoms in direct contact with residue 210 is improved by the mutation as small internal cavities and surface pockets are either eliminated or reduced (Fig. 2, upper panel).

Changes induced by the mutation at position 229 are shown in Figure 1, panel B. The rings of Trp 229 and Phe 229 are in similar planes. The side chains closer to the mutation adopt similar rotamers in both wild-type and mutant lactamases, and the backbone dihedrals do not change significantly. Mutant and wild-type packing of atoms contacting residue 229 are similar, however the mutation causes a movement of the C-terminus and a consequent enlargement of a surface pocket on the edge of the aromatic ring (Fig. 2, middle panel).

The benzene rings are superimposed after the mutation at position 251 (Fig. 1, panel C). To achieve this, the side chain moves inward 1.4 Å pushed by a rigid body movement of the backbone segment 250-253. As a result of the movement, the region becomes somewhat more compact. The solvent exposure of residue 251 increases 1.2% in the mutant, but the surrounding residues decrease their exposure by 2%. Accordingly, the volumes of small cavities and pockets in direct contact with residue 251 are comparable in the wild-type and mutant protein (Fig. 2, lower panel).

Effects of the mutations on the active site

Catalytic parameters derived from Michaelis–Menten curves for benzylpenicillin and nitrocefin are given in Table III. The cephalosporin nitrocefin is bulkier than penicillins and therefore is hydrolyzed less efficiently by β-lactamases. The values determined for ESP are in good agreement with the literature.[24–27] The effects of the mutations are similar for the two substrates: a slight increase in K_M, a ~50% diminished k_{cat} , and an about three times lower k_{cat}/K_M. The inspection of the active site (Fig. 3) revealed no significant differences between $ESP^{\Delta W}$ and the rest of lactamases listed in Table II. All the catalytically important atoms occupy the canonical positions. Among these, two conserved water molecules are seen in the substrate binding pocket of $ESP^{\Delta W}$ and there is electron density for a citrate moiety, which has been reported before for lactamases crystallized in its presence. Thus, the moderate alteration in the catalytic parameters cannot be attributed to gross conformational changes in the active site (Fig. 3) and probably it is related to differences in residue packing and/or dynamics effects. Indeed, the interatomic distances of atoms within 5.0 Å of Ser 70 and interacting through van der Waals and hydrogen bonds are, on average, shorter in $ESP^{\Delta W}$ than in ESP ($\Delta = 0.15 \pm 0.016$ Å; *mean* ± SEM; $n = 98$). A subset of ten of these distances corresponding to atoms believed to be directly involved in catalysis or substrate binding are on average 0.19 Å shorter in $ESP^{\Delta W}$. Particularly noteworthy are the distances between Glu 166 OE2–Ser 70 OG and Ala 237 N–Ser 70 OG, which are 0.5 and 0.4 Å shorter, respectively, in $ESP^{\Delta W}$. The displacement of Glu 166 is the result of an inward movement of the Ω loop (residues 162 to 170). One of the consequences of this movement is probably the alteration in the conformation of residues 102 and 103 mentioned above. In addition, the "hydrolytic" water molecule (Fig. 3), which is considered to participate in the deacylation of the acyl–enzyme intermediate during catalysis, is

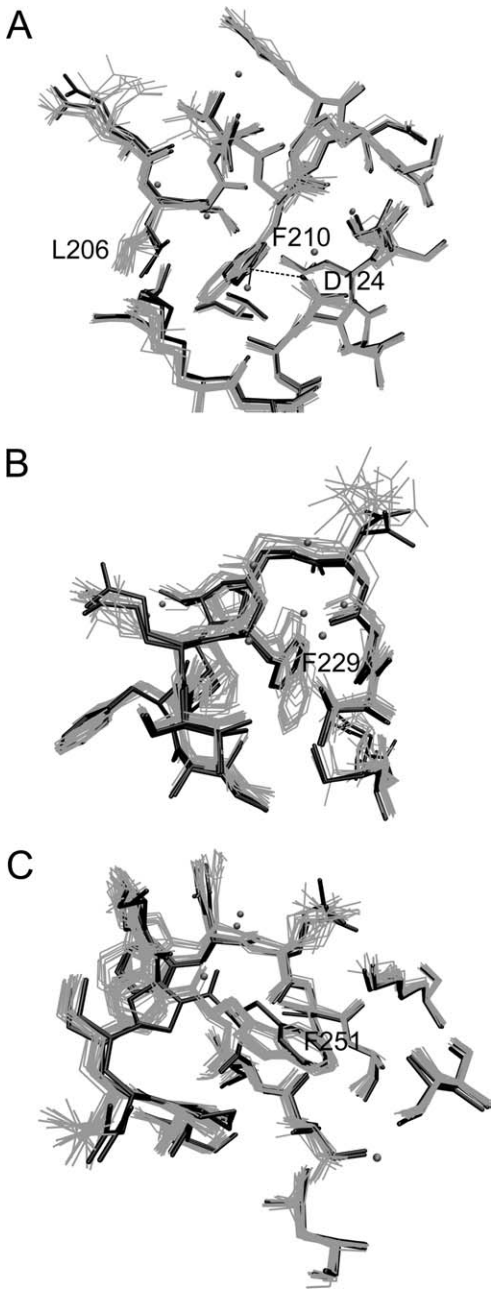

Figure 1. Local changes induced by the mutation Trp →Phe. The structures of thirteen *B. licheniformis* β-lactamases (see Table II) are shown in light gray. $ESP^{\Delta W}$ is represented in dark gray. For clarity, only the water molecules of $ESP^{\Delta W}$ have been represented (spheres). Panel A shows residues within 6.0 Å of Phe 210. Leu 206 adopts a different rotamer in $ESP^{\Delta W}$, and because of the mutation, the hydrogen bond between Trp 210 NE1 and Asp 124 OD2 atoms can no longer form (dashes). Interestingly, a conserved water molecule, at proper distance and angle for hydrogen bonding to Trp 210 NE1, is preserved in the mutant, as if it were hydrogen-bonded to Phe 210 CE1. In Panel B, residues within 6.0 Å of Phe 229 are represented. In this case, the mutation has little effects on the conformation of the surroundings. Residues close to residue 251 are shown in Panel C. The mutated side chain moves inward following a rigid body movement of the backbone of residues 249–253.

displaced toward the Glu OE2 and away from Ser 70 OG in $ESP^{\Delta W}$ (0.4 and 0.6 Å, respectively).

Overall packing effects

By visual inspection of the superimposed structures, $ESP^{\Delta W}$ impresses as being more compact than its cognates in Table II. A closer scrutiny showed that the radius of gyration (R_g) of 1021 backbone atoms is significantly smaller in $ESP^{\Delta W}$ than in the other lactamases: 16.77 Å versus 17.09 ± 0.07 Å (*mean* ± SEM; Table II). The compared structures are from 749/C and BS3 Class-A lactamases, which differ at seven positions in sequence, have been crystallized at different pH, and whose temperature of X-ray data collection varied from cryogenic to room temperature. However, none of these factors seem obviously related to the 0.32-Å difference in R_g calculated for $ESP^{\Delta W}$.

The above result prompted us to calculate the R_g of all the other Class-A lactamases structures deposited in the PDB. To that end, all the positive hits of a Blast search using the $ESP^{\Delta W}$ sequence as a

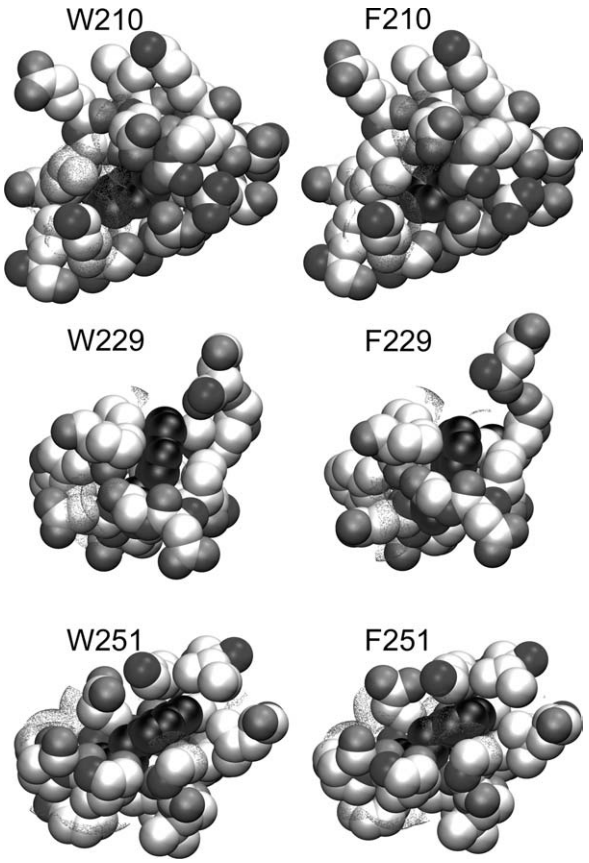

Figure 2. Cavities and surface pockets in the vicinity of the mutated tryptophan residues. The van der Waals representations of ESP atoms (PDB ID: 4BLM) are on the left. Equivalent representations are shown on the right for $ESP^{\Delta W}$. Dots show surfaces that belong to crevices or cavities as calculated by the CASTp server (see Materials and Methods). Mutated residues are shown in black; all other atoms are shown in shades of gray.

Table III. *Catalytic Properties of ESP and ESP$^{\Delta W}$*

Substrate	Variant	k_{cat} (s^{-1})	K_M (M)	k_{cat}/K_M (s^{-1} M^{-1})
Benzylpenicillin	ESP[16]	3060 ± 13	$1.8 \pm 0.5 \times 10^{-4}$	1.7×10^7
	ESP[27]	2200	7.6×10^{-5}	2.3×10^7
	ESP[25]	2650	1.2×10^{-4}	2.1×10^7
	ESP[28]			2.9×10^7
	ESP$^{\Delta Wa}$	1540 ± 60	$2.6 \pm 0.1 \times 10^{-4}$	5.9×10^6
Nitrocefin	ESP[1]	564 ± 44	$3.8 \pm 0.6 \times 10^{-5}$	1.5×10^7
	ESP[27]	470	3.8×10^{-5}	1.3×10^7
	ESP[25]	1088	4.1×10^{-5}	2.7×10^7
	ESP$^{\Delta W\ 1}$	221 ± 20	$4.8 \pm 0.5 \times 10^{-5}$	4.6×10^6

[a] Average of two to three measurements ± SEM.

query were filtered for incomplete or very divergent number of backbone atoms. The search provided 126 structures from several different bacterial strains having between 1017 and 1025 equivalent backbone atoms. The average R_g of this set of structures is 17.10 ± 0.09 Å (*mean* ± SEM) and the smallest value found in the distribution was 16.91 Å (PDB ID: 1djc). Thus, the R_g of ESP$^{\Delta W}$ is 0.15 Å smaller than the smallest R_g of all comparable lactamase structures in the PDB. This is a remarkable result because the 126 lactamases in the control set have a very narrow distribution of Rg values, despite differing greatly in sequence and experimental conditions.

To get a deeper insight into the change that causes the R_g difference, every backbone atom distance to the geometric center of the molecule was calculated, and the difference between these values and the averages for the *B. licheniformis* lactamases were compared. As expected from the R_g data, the results of such calculation indicate that most backbone atoms in ESP$^{\Delta W}$ are closer to the center than average (Fig. 4). To visualize the spatial variation of the distances to the center differences, a cartoon representation of ESP$^{\Delta W}$ was colored using a scale from blue to red (Fig. 5). The representation indicates that the shrinkage affects most of the protein matrix, being the central and interdomains regions the least affected. Very similar results were obtained

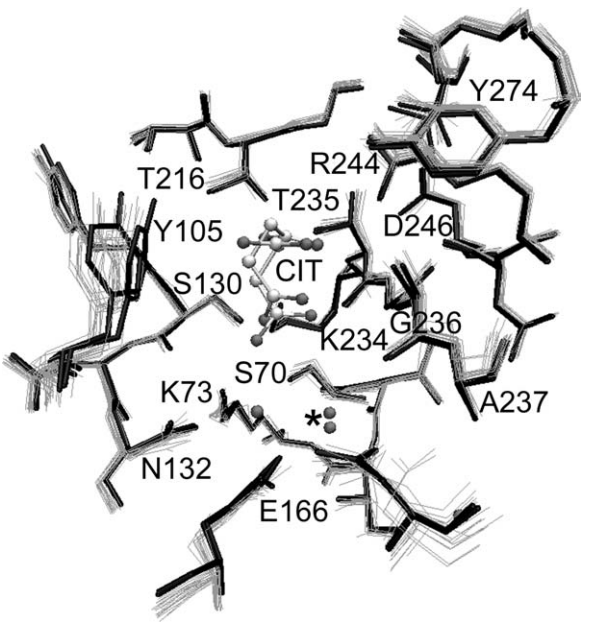

Figure 3. The active site of ESP$^{\Delta W}$ and other *B. licheniformis* β-lactamases. Atoms of residues within 6.0 Å of Ser 70 (the residue that forms a transient covalent complex with the substrate during catalysis) from ESP$^{\Delta W}$ (dark sticks, for chain A and B) and the thirteen lactamases (gray lines) listed in Table II are superimposed. Some of the residues that are relevant for catalysis or substrate binding have been labeled. Citrate in ESP$^{\Delta W}$ is shown (CIT). Water in the ESP$^{\Delta W}$ structure is shown as spheres. An asterisk marks the position of the so called "hydrolytic water" present in many lactamase structures and deemed responsible for the nucleophilic attack to the acyl–enzyme during catalysis.

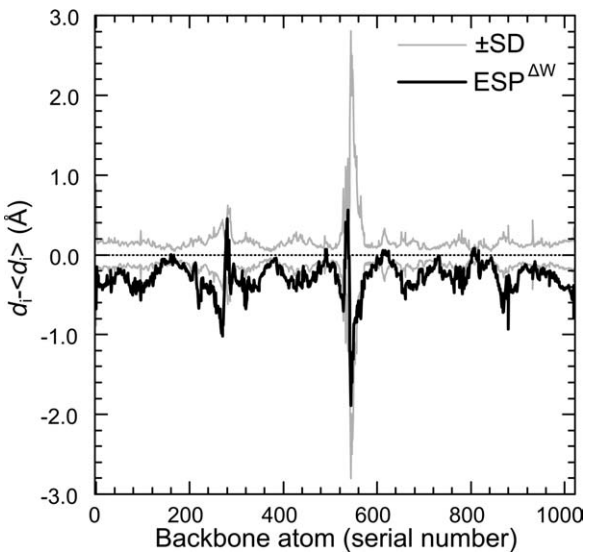

Figure 4. Normalized distances to the geometric center. The average $\langle d_i \rangle$ and standard deviation (SD_i) of the distances of each backbone atom i to the respective geometric center of the molecule were calculated for the lactamases in Table II. The deviation from the average $d_i - \langle d_i \rangle$ in the ESP$^{\Delta W}$ structure is shown as a bold line. The $\pm SD_i$ boundaries are shown as gray lines. The central peak in the plot with the largest SD variation corresponds to the Ω loop, a very mobile region known to be of central importance in the catalytic mechanism of lactamases.

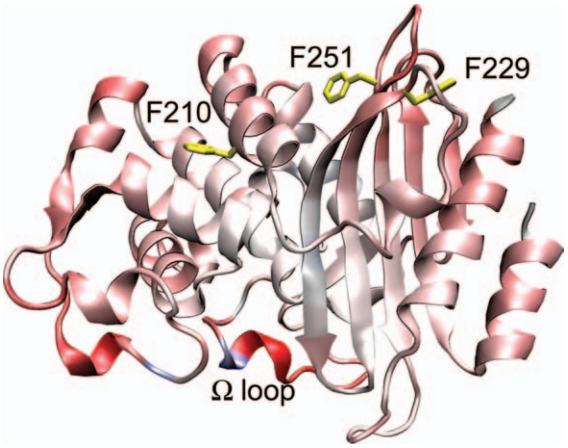

Figure 5. Color coded distance shift in ESP$^{\Delta W}$. The d_i–$\langle d_i \rangle$ values shown in Figure 4 were used to generate a linear color scale from red (−1.0 Å) to white (0.0 Å) and white to blue (1.0 Å). Thus, backbone atoms closer to the geometric center than in the average lactamases are colored in shades of red; whereas those farther than average from the center appear bluish. ESP$^{\Delta W}$ mutations are shown in yellow.

comparing the distances to the average of *B. licheniformis* structures or to the structure of wild–type ESP alone (PDB ID: 4BLM; not shown). As the latter structure and ESP$^{\Delta W}$ have the same sequence (except for the Trp→Phe mutations), further detailed comparisons were carried out adopting the 4blm PDB entry as the wild-type ESP reference structure.

To further characterize the conformational rearrangements occurring in ESP$^{\Delta W}$, a RMSD superposition to the coordinates of ESP was performed. The fit was restricted to the ESP$^{\Delta W}$ backbone atoms with low changes in distance to the geometric center (the "white cluster" in the center of Fig. 5). The result of the superposition is shown in Figure 6. Displacement vectors indicate that many regions of the molecule undergo rigid-body movements toward the center and toward each other. The most striking movements are: a squeezing of the helices of the α + β domain against the central five-stranded β-sheet; a tilt of loops 51–54, 225–231, and 254–257 toward the center of the α + β domain, a displacement of the β-sheet toward the α domain, and a movement of most of the α-domain elements toward the interface between domains and toward the center of the domain.

The widespread movements of the ESP$^{\Delta W}$ atoms toward the center or toward each other explain the decrease in R_g described above and suggest that the lactamase variant possesses an overall better packing than the wild-type protein. To confirm this, the number of atoms in fixed volumes of both proteins was measured. This was accomplished counting the atoms in spheres of 10-Å radius centered at each CA atom. The percentage difference between ESP$^{\Delta W}$ and ESP is plotted in Figure 7. The result shows that most regions are in a more compact state in ESP$^{\Delta W}$ than in the wild-type ESP.

The packing improvement prompted us to compare the noncovalent interactions in ESP$^{\Delta W}$ and the wild-type protein. To that end, two atoms separated by less than 5.0 Å and apart in protein sequence by

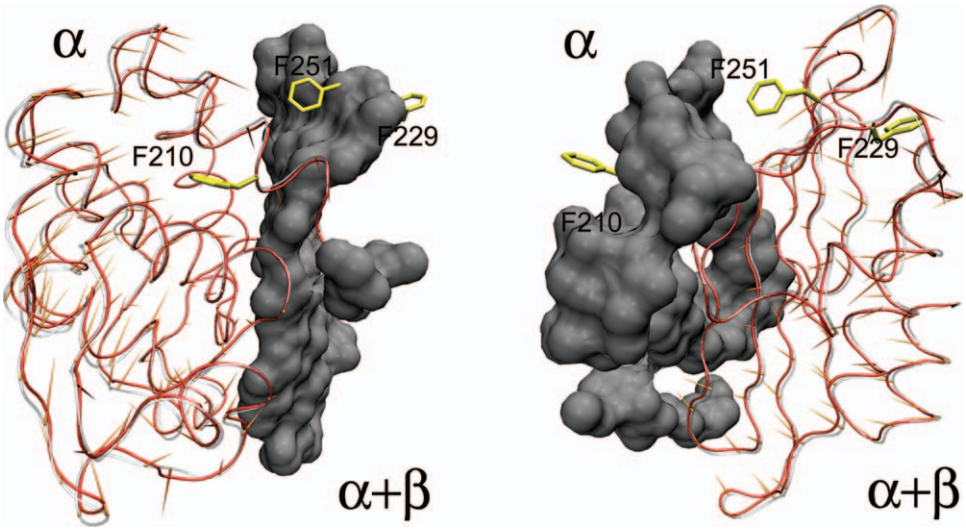

Figure 6. Concerted shifts of backbone atoms. The coordinates from ESP$^{\Delta W}$ and wild-type ESP (PDB ID: 4BLM) were superimposed to minimize the RMSD of the backbone atoms shown in white in Figure 5 (residues 70 to 73, 183 to 190, and 233 to 236), which do not move significantly toward the geometric center. On the left, the α + β domain backbone is represented as a wire in contact with nearby atoms of the α domain (solid surface). On the right, the representation is reversed (i.e., the α domain is a wire and the close by atoms in domain α + β are drawn as a solid surface). For clarity, the orientation is slightly different in both panels. The red and gray wires correspond to ESP$^{\Delta W}$ and wild-type ESP coordinates, respectively. Vectors showing the displacements of the positions of equivalent atoms in the two structures are represented as orange spines (scaled by a factor of 5 to better visualize the directions).

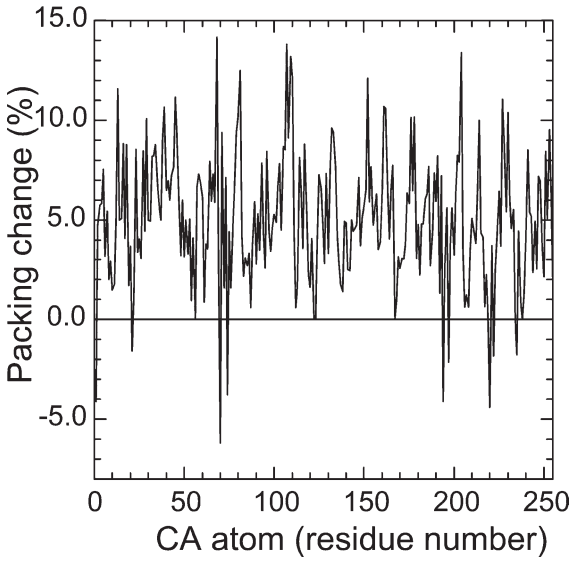

Figure 7. Atom density differences. The atoms in spheres of 10-Å radius centered at each CA atom were counted, and the percentage difference between $ESP^{\Delta W}$ and ESP is shown in the plot.

three or more residues were considered a noncovalent interaction. There are more of such interactions in $ESP^{\Delta W}$ than in wild-type ESP (9319 vs. 8370, respectively). The mean and SEM of these distances are 4.282 ± 0.005 and 4.309 ± 0.006 Å for $ESP^{\Delta W}$ and ESP, respectively ($P < 4 \times 10^{-4}$). Moreover, plotting the distance differences in the form of contact maps showed that the shorter noncovalent interactions are evenly distributed all over the structure (Fig. S1; Supporting Information).

Similar results are obtained considering only those noncovalent interactions mediated by hydrogen bonds. In this case, the average hydrogen-bond distance in $ESP^{\Delta W}$ and the wild-type protein is 2.967 ± 0.012 (±SEM, $n = 463$) and 3.045 ± 0.013 Å (±SEM, $n = 470$), respectively ($P < 10^{-5}$). These figures can be further compared with 3.050 ± 0.004 Å (±SEM, $n = 4893$), the value obtained for the lactamases listed in Table II (excluding $ESP^{\Delta W}$). Thus, although it might seem small, the difference (−0.08 Å) between $ESP^{\Delta W}$ and the other *B. licheniformis* lactamases is highly significant ($P < 10^{-10}$).

Although the noncovalent interactions examined above are crucial for protein conformation and stability, they account for only a small fraction of the difference in the packing and R_g between wild-type and $ESP^{\Delta W}$. When the 5.0 Å limit is removed and all distances are considered, it becomes apparent that the entire distance distribution is shifted toward lower values in $ESP^{\Delta W}$ compared with the wild type molecule (not shown).

The generalized decrease of interatomic distances observed for $ESP^{\Delta W}$ raised the question whether the main internal pockets and cavities were remodeled by the mutation. There are two main surface pockets and one internal cavity in wild-type ESP. The Ω loop contributes to the formation of these three voids, which are located at the antipodes of the sites of mutations. The first surface pocket occupies ~290 $Å^3$, is formed by the top of the five-stranded β-sheet and four surface loops, and is filled with 6-9 water molecules. The importance of this pocket in shaping the active site of the lactamases was recognized very early,[28] and its volume and shape are similar in $ESP^{\Delta W}$ and ESP (not shown). The second pocket is next to the first, underneath the C- and N-terminal helices, it contains four water molecules and its volume is 131 and 102 $Å^3$ in ESP and $ESP^{\Delta W}$, respectively. The third, internal cavity is adjacent to the first pocket, contains three water molecules hydrogen-bonded to the backbone, and is 75 $Å^3$ in the wild-type protein and 59 $Å^3$ in the mutant. Inspection of the remainder and less prominent internal cavities revealed that these are fewer and smaller in the mutant than in the wild-type protein (Fig. S2; Supporting Information).

The subtle movements within the matrix of $ESP^{\Delta W}$ have no impact on other general properties of the structure, such as for instance the B-factors. The backbone B-factors in $ESP^{\Delta W}$ are similarly low, or even lower, than in ESP. Thus, a significant effect of the mutations on the mobility of the atoms in the crystal of $ESP^{\Delta W}$ was discarded.

Thermodynamic effects of the mutation

The effect of tryptophan replacement on the stability of ESP and $ESP^{\Delta W}$ was assessed by equilibrium thermal unfolding, monitoring the ellipticity at 220 nm (i. e., the secondary-structure content) as a function of temperature. The wild-type protein and the mutants unfolded reversibly, with more than 95% percent recovery of the original signal upon cooling (not shown). Thus, the equilibrium condition was assumed for the analysis, and the corresponding thermodynamic parameters were derived from the thermal transitions using a two-state model to fit the data (Table IV). The ΔCp value for ESP was close to 4 kcal mol^{-1} K^{-1}, which is compatible with the expected increase of exposed area upon unfolding[29] and with the value obtained for this protein in differential scanning calorimetry experiments (V. A. Risso and M. R. Ermácora, unpublished results). The ΔCp value for the mutant is somewhat lower, which may indicate a difference in the states populated by this variant during unfolding. $ESP^{\Delta W}$ exhibits the characteristic pH dependence of T_m and ΔH_{Tm} reported before for ESP.[15] $ESP^{\Delta W}$ is 1.8 kcal mol^{-1} less stable than ESP at the temperature of maximum stability. At 25°C, the calculated difference in stability is of 2.3 kcal mol^{-1}. In a previous work, it was found that the $W_{210} \rightarrow F$ substitution alone destabilizes ESP by approximately 1.5 kcal mol^{-1} and that the same substitutions at position

Table IV. *Thermal Unfolding Parameters*[a]

Variant	pH	T_m[b] (°C)	ΔH_{Tm} (kcal mol^{-1})	ΔC_P (kcal mol^{-1} K^{-1})	T_{max}[b] (°C)	ΔG_{Tmax} (kcal mol^{-1})	$\Delta H_{25°C}$ (kcal mol^{-1})	$\Delta G_{25°C}$ (kcal mol^{-1})	$T\Delta S_{25°C}$ (kcal mol^{-1} K^{-1})
ESP	6.0	68.8 ± 0.1	147.1 ± 0.4	3.91 ± 0.05	32.9	7.1	−23.9	6.7	−30.7
	7.0	66.9 ± 0.1	139.9 ± 0.5						
	8.0	65.1 ± 0.1	132.8 ± 0.5						
ESP$^{\Delta W}$	6.0	65.7 ± 0.1	111.5 ± 0.3	3.32 ± 0.05	33.7	5.3	−21.0	4.4	−25.4
	7.0	62.8 ± 0.1	104.7 ± 0.3						
	8.0	60.5 ± 0.1	98.9 ± 0.3						

[a] Unfolding transitions as a function of temperature were monitored by CD at 220 nm, and the unfolding curves were analyzed as described in Materials and Methods.
[b] T_m and T_{max} are the temperatures of melting ($\Delta G = 0$) and maximum stability (ΔG maximum), respectively. The errors were calculated by performing four fits with one quarter of equally spaced data points each time and averaging the results.

229 and 251 account for an additional stability loss of circa 0.5 kcal mol^{-1} each.[16] Thus, the stability loss in the triple mutation reported herein is roughly additive and in the order of 0.25 kcal per buried methylene eliminated.

Discussion

The native state of ESP$^{\Delta W}$ could be characterized at high resolution by X-ray diffraction providing an opportunity to scrutinize the conformational mechanisms that compensate the energetic cost of unfavorable side chain mutations. Based on strictly geometric considerations, the tryptophan to phenylalanine substitutions would be expected to have strongly destabilizing effects. The cavities around the mutated residues detected using a 1.4 Å probe would increase ~70 Å^3 if the rest of the structure remained static, and the removal of nine carbon atoms would cause a large reduction of contacts and packing density. However, the mutations cause only a modest total destabilization of ~2 kcal mol^{-1}. This value is very small taking into account that the energetic cost of removing a single methylene group from a buried hydrophobic side chain in a protein interior has been estimated as 1.2–1.5 kcal mol^{-1}.[30–32] Thus, an important structural adjustment must be taking place, to allow ESP$^{\Delta W}$ to tolerate the mutations at such a low energetic cost.

Notwithstanding its evident effects in the stability, the structural rearrangement is not readily apparent by a conventional examination of the structure. A comparison between ESP$^{\Delta W}$ and other closely related *B. licheniformis* lactamases using criteria, such as RMSD, or Ramachandran plots, reveals little that could be interpreted as a qualitative change in secondary or tertiary structure. Only a rotamer shift populated by Leu 206, close to the replaced Trp 210, may qualify as a specific conformational effect of the mutations. However, a closer scrutiny using different criteria revealed that the main conformational effect of the mutations is of a more general and subtle nature and consists in a concerted movement of nearly the entire backbone toward the geometric center of the molecule.

Although visual comparison of superimposed structures gives a hint of the molecular shrinkage, this striking effect is readily detected by R_g and other atomic density measurements. R_g, a measure of the atomic distribution relative to the mass center, is particularly sensitive to the change because it has a very narrow probability distribution among the 126 Class-A β-lactamases analyzed herein, and therefore the departure from the average allows a clear distinction of ESP$^{\Delta W}$. The average number of atoms within a standard spherical volume centered at each CA position is also a clear discriminator between ESP$^{\Delta W}$ and the lactamases in the *B. licheniformis* group.

The atypical interatomic distance distribution in ESP$^{\Delta W}$ involves all the structural levels but the covalent bonds. Hydrogen bonds, van der Waals interactions, and other larger through-space distances are on average shorter in ESP$^{\Delta W}$ and also more numerous. The analysis showed that most ESP$^{\Delta W}$ atoms are closer to the molecular center as a result of the inward movement of nearly all the backbone segments. The transformation is more isotropic than what would result from a local backbone bending or hinge movement such as that observed in the open-closed forms of allosteric proteins.

The rearrangement observed in ESP$^{\Delta W}$ structure resembles that induced in other proteins by temperature or pressure changes,[33–35] but it is of a greater magnitude. For instance, data compiled by Rader and Agard[36] showed that for α-lytic protease, trypsin, ribonuclease-A, hen egg white lysozyme, and myogobin R_g decreases by 0.13–1.04% when X-ray diffraction is from crystals at cryogenic temperature (~100 K). Additionally, we calculated that in the set of 30 proteins pairs studied by Fraser[37] the average R_g contraction caused by cryocooling is 0.4 ± 0.1% (Ermácora, M. R. unpublished results). On the other hand, high pressure causes R_g changes similar to that of cryocooling.[38] The compression of ESP$^{\Delta W}$ inferred from the R_g value is 1.9%, twofold to threefold higher than expected if a temperature or pressure change were the causal factor.

An exploratory search among several archetypal proteins measuring R_g, packing density and noncovalent interactions (Ermácora *et al.*, unpublished

results) suggests that increased compactness is very rare. For instance, among the over four hundred T4 lysozyme mutants characterized in the remarkable work by Matthews's group[21] we found a handful of cases with a significant reduction of R_g, but none with the characteristics described herein for ESP$^{\Delta W}$. Indeed, engineered disulfide bridges, or multiple mutations can cause up to 2% reduction in the R_g of T4 lysozyme, but this does not result in a significant shortening of the average short-range interactions or in the improvement of the average atomic packing. Rather, in these cases, the change can be ascribed to large hinge-bending movements of entire domains, which move toward to each other without much effect in their internal compactness.

Among the other archetypal proteins examined in the exploratory search we found only two examples of statistically significant R_g contraction accompanied by improved packing and shortening of noncovalent interactions: a staphylococcal nuclease core mutant (PDB ID: 2SNM) and a trypsin-ligand complex (PDB entry 3GY3). Very interestingly, the contraction in the trypsin complex seems to be induced by the ligand, and a series of liganded structures are available[39] which suggest that the effect may be related to the extent of the protein–ligand interaction.

As the global degree of compactness is generally accepted as a strong determinant of protein stability, it would be expected that native structures had the greatest compactness allowed for a given fold and state. Exceptions are known, but generally they are associated with expanded states, in which the loss of tight tertiary interactions is thought to be energetically counterbalanced by the entropic gain due greater side chain mobility. The results presented herein show that the degree of compaction can vary also in the opposite direction, that is, toward structures more densely packed than the native state. For these cases, we propose that the entropic cost of more restricted side chain mobility would disfavor the native state but the effect is compensated by stronger and more abundant noncovalent interactions.

As expected, the modeling exercise of reintroducing the original tryptophan side chains in the context of ESP$^{\Delta W}$ structure reveals that only local conflicts are created by the bulkiness of the indolyl moiety (not shown). These local defects are mostly steric clashes with backbone atoms and can be alleviated by a simple readjustment of side chain dihedral angles and minor backbone shifts. Thus, the question arises as to what deters the wild type structure to adopt preferentially a more compact state that would result in stronger and more abundant noncovalent interactions. Inspecting the changes that would be necessary to fit the tryptophan residues in the ESP$^{\Delta W}$ context it becomes clear that in the adjusted structure the local rotamer's conformational freedom is significantly restricted by crowding. Thus, in the case of the wild-type protein, we propose that the more compact native state is energetically disfavored for entropic reasons.

Implicit in the above suggestion is that the less costly solution to the local conflict between the tryptophan side chains and the compact state involves a global expansion. In other words, in the wild-type structure, making room for the tryptophan residues is more efficiently achieved by expanding the entire molecule rather than the tryptophan's surroundings, as if the tryptophan residues of ESP were wedges placed at critical points and able to displace outwardly most of the backbone atoms.

Cavity creating mutations like those described herein have been given a considerable attention before.[17,20,40–45] In general, proteins react parsimoniously to such changes. Voids are tolerated or either minimized by small scale and local backbone shifts. Repacking the environment of the mutated residues by varying the rotamer selection seems to be seldom utilized.[23,46] ESP$^{\Delta W}$ illustrates an alternative, and previously unnoticed, strategy to fill the voids and maintain the number and strength of van der Waals interactions. This strategy is also very conservative in terms of preserving qualitatively the backbone and side chain dihedral angles. However, it resorts to a general fine tuning of the backbone conformation to achieve a global shrinkage of the structure. As a consequence of the readjustment, the entire matrix is better packed. A simple explanation for the global character of the structure reaction to the mutations is that, unlike most cases described in the literature of core mutants, the changes in ESP$^{\Delta W}$ are in three separated spots of the protein matrix. Moreover, these places map critical structural elements: Trp 210 and Trp 251 are associated to the α and α+β domains, respectively; whereas Trp 229 mediated the interaction between the two domains. Hence, it is conceivable that, acting in concert, local backbone shifts at each of these regions are better accommodated in the context of a generalized shrinkage of the entire protein.

Finally, the increase in the density of packing in ESP$^{\Delta W}$ is clearly evidenced in the enzyme active site. Although there are no differences in residue and backbone conformation at the active site between the wild-type and mutated lactamase, in the latter almost all the interatomic distances are shorter. Particularly, several atoms directly involved in catalysis are closer to each other by as much as 0.4–0.5 Å. Crowding at the active site affects catalysis increasing K_M and lowering k_{cat}. This is not surprising because it is well known that mechanical flexibility at the active site is positively correlated with catalytic efficiency.[47] Interestingly, the other factor positively correlated with catalytic efficiency is a decrease in thermodynamic stability, because highly stable protein structures are less flexible. As ESP$^{\Delta W}$ combine both, active site

crowding and decreased stability, it may become a very useful model to test current ideas on molecular evolution and catalysis. Incidentally, this trade-off between fitness for function and compactness might be the explanation for the fact that all other lactamases examined herein have less density of packing than ESP$^{\Delta W}$.

In summary, this work establishes a new lower limit for the compactness associated to the Class-A β-lactamase fold and suggests that the compactness of the native state may be increased by removing bulky side chains that restrain the inward displacement of the backbone. As the degree of condensation achieved by the native state is a paramount notion in the protein folding theory, the result may contribute to better understanding of how the sequence determines the conformational variability and thermodynamic stability of a given fold. The observations reported herein will help in the design of new studies aimed to test whether the compactness of the native state is under evolutionary pressure and also provide new useful information for protein engineering and drug design.

Materials and Methods

General details

Benzylpenicillin was purchased from Sigma (St. Louis, Missouri). Nitrocefin (NC) was from Calbiochem. Protein purity was assessed by SDS-PAGE. Circular dichroism (CD) and analytical size-exclusion chromatography were carried out as described.[11] ESP$^{\Delta W}$ is a triple Trp→Phe mutant of ESP (UniProt ID: P00808, E.C. = 3.5.2.6), and its preparation was described previously.[16] Enzymatic activity was determined spectrophotometrically at 25 °C in 50 m*M* sodium phosphate, pH = 7.0 supplemented with 1.5 μM bovine serum albumin and the desired concentration of benzylpenicillin ($\Delta\varepsilon_{240\ nm}$ = 570 M^{-1} cm^{-1})[48] or nitrocefin ($\Delta\varepsilon_{486\ nm}$ = 20,500 M^{-1} cm^{-1}). Molecular visualization, analysis, and most structural alignments were performed using VMD[49] Accessible surface area was calculated with a 1.4 Å probe. Contact maps were calculated using in-house C-code for measuring every distance between atoms $\mathbf{r}_{ik}$-$\mathbf{r}_{jl}$, were i and j are atom serial numbers, k and l are residue numbers, and $|k\text{-}l| > 2$. Ambler residue numeration was used throughout.[50] The number of atoms within a 10 Å sphere centered at each CA atom was obtained using a tcl script running in VMD. Internal cavities and surface pockets were calculated using the CASTp server[51] and a 1.4-Å probe. Reported volumes calculated by CASTp are molecular surface volumes.

Crystallographic procedures

Crystals of ESP$^{\Delta W}$ were obtained after two weeks at 19 °C by the hanging drop method. The reservoir solution (300 μl) was 28% PEG 4000, 0.1 M sodium citrate, pH = 5.4. The drop (2 μl) was a 1:1 blend of reservoir and protein solutions (10 mg/ml in 10 m*M* Tris-HCl, 50 m*M* NaCl, pH = 7.0). x-ray diffraction data were collected at the D03B-MX1 protein crystallography beamline of the Laboratorio Nacional de Luz Síncrotron, Campinas, Brazil. Data reduction and processing were carried out with the programs MOSFLM and Scala (CCP4 suite). Crystals belong to the space group $P2_1$, with unit cell parameters $a = 42.8$, $b = 110.1$, $c = 54.1$ Å, $\alpha = 90.00$, $\beta = 89.97$, $\gamma = 90.00°$. Two molecules are present in the asymmetric unit. Relevant data collection parameters are given in Table I.

Structure determination and refinement

The ESP$^{\Delta W}$ structure was solved by molecular replacement with the AMoRe package,[52] using the coordinates for ESP (PDB ID: 4BLM) as a search model. Refinement was carried out using REFMAC 5.[53] Coot[54] was used for model inspection and rebuilding. The model was refined to final R_{factor} = 17.1% and R_{free} = 19.3%. Further details of crystallization, data collection, processing, and refinement can be found in Table I. The final model was validated using PROCHECK.[56]

Thermal unfolding

Unfolding transitions as a function of temperature were monitored by CD at 220 nm with a 1.0-cm cell. Protein concentration was 1.5 μ*M*, and the temperature was varied linearly from 0 to 95°C at a 2°C min^{-1} rate. The following equations were used in the data fit[55]

$$\Delta G_{NU} = -RT\ \ln\left(\frac{f_U}{f_N}\right) = \Delta H_{Tm} + \Delta C_p(T - T_m) - T\left[\left(\frac{\Delta H_{Tm}}{T_m}\right) + \Delta C_p \ln\left(\frac{T}{T_m}\right)\right] \quad (1)$$

and

$$S = f_N(S_{0,N} + l_N T) + f_U(S_{0,U} + l_U T), \quad (2)$$

where f_U and f_N are the unfolded and folded fractions at equilibrium and f_U+f_N = 1, T_m is the temperature at which $f_U = f_N$, S is the observed CD signal, $S_{0,N}$ and $S_{0,U}$ are the intrinsic CD signals for the native and unfolded state, respectively, l_N and l_U are the slopes for the assumed linear dependence of $S_{0,N}$ and $S_{0,U}$ with the temperature. CD buffer was 25 m*M* sodium phosphate, 100 m*M* sodium fluoride. The fit was performed simultaneously for pH = 6.0, 7.0, and 8.0, with a global ΔC_P and pH-specific energy and baseline parameters.

Acknowledgments

The authors are grateful to the staff of the Facility LNLS Laboratorio de luz Sinchroton in Campinas, SP, Brazil for assistance during data collection.

References

1. Strynadka NC, Adachi H, Jensen SE, Johns K, Sielecki A, Betzel C, Sutoh K, James MN (1992) Molecular structure of the acyl-enzyme intermediate in beta-lactam hydrolysis at 1.7 A resolution. Nature 359: 700–705.
2. Escobar WA, Tan AK, Lewis ER, Fink AL (1994) Site-directed mutagenesis of glutamate-166 in beta-lactamase leads to a branched path mechanism. Biochemistry 33:7619–7626.
3. Jamin M, Damblon C, Bauduin-Misselyn AM, Durant F, Roberts GC, Charlier P, Llabres G, Frere JM (1994) Direct n.m.r. evidence for substrate-induced conformational changes in a beta-lactamase. Biochem J 301: 199–203.
4. Lewis ER, Winterberg KM, Fink AL (1997) A point mutation leads to altered product specificity in beta-lactamase catalysis. Proc Natl Acad Sci USA 94: 443–447.
5. Lietz EJ, Truher H, Kahn D, Hokenson MJ, Fink AL (2000) Lysine-73 is involved in the acylation and deacylation of beta-lactamase. Biochemistry 39:4971–4981.
6. Creighton TE, Pain RH (1980) Unfolding and refolding of Staphylococcus aureus penicillinase by urea-gradient electrophoresis. J Mol Biol 137:431–436.
7. Thomas RM, Feeney J, Nicholson RB, Pain RH, Roberts GC (1983) Identification by n.m.r. spectroscopy of a stable intermediate structure in the unfolding of staphylococcal beta-lactamase. Biochem J 215:525–529.
8. Goto Y, Fink AL (1989) Conformational states of beta-lactamase: molten-globule states at acidic and alkaline pH with high salt. Biochemistry 28:945–952.
9. Ptitsyn OB, Pain RH, Semisotnov GV, Zerovnik E, Razgulyaev OI (1990) Evidence for a molten globule state as a general intermediate in protein folding. FEBS Lett 262:20–24.
10. Frate MC, Lietz EJ, Santos J, Rossi JP, Fink AL, Ermácora MR (2000) Export and folding of signal-sequenceless *Bacillus licheniformis* beta-lactamase in *Escherichia coli*. Eur J Biochem 267:3836–3847.
11. Santos J, Gebhard LG, Risso VA, Ferreyra RG, Rossi JP, Ermácora MR (2004) Folding of an abridged beta-lactamase. Biochemistry 43:1715–1723.
12. Gebhard LG, Risso VA, Santos J, Ferreyra RG, Noguera ME, Ermacora MR (2006) Mapping the distribution of conformational information throughout a protein sequence. J Mol Biol 358:280–288.
13. Santos J, Risso VA, Sica MP, Ermácora MR (2007) Effects of serine-to-cysteine mutations on beta-lactamase folding. Biophys J 93:1707–1718.
14. Ureta DB, Craig PO, Gomez GE, Delfino JM (2007) Assessing native and non-native conformational states of a protein by methylene carbene labeling: the case of *Bacillus licheniformis* beta-lactamase. Biochemistry 46: 14567–14577.
15. Risso VA, Primo ME, Ermácora MR (2009) Re-engineering a beta-lactamase using prototype peptides from a library of local structural motifs. Protein Sci 18: 440–449.
16. Risso VA, Primo ME, Brunet JE, Sotomayor CP, Ermacora MR (2010) Optical studies of single-tryptophan *B. licheniformis* beta-lactamase variants. Biophys Chem 151:111–118.
17. Eriksson AE, Baase WA, Zhang XJ, Heinz DW, Blaber M, Baldwin EP, Matthews BW (1992) Response of a protein structure to cavity-creating mutations and its relation to the hydrophobic effect. Science 255:178–183.
18. Anderson DE, Hurley JH, Nicholson H, Baase WA, Matthews BW (1993) Hydrophobic core repacking and aromatic-aromatic interaction in the thermostable mutant of T4 lysozyme Ser 117-->Phe. Protein Sci 2: 1285–1290.
19. Buckle AM, Henrick K, Fersht AR (1993) Crystal structural analysis of mutations in the hydrophobic cores of barnase. J Mol Biol 234:847–860.
20. Buckle AM, Cramer P, Fersht AR (1996) Structural and energetic responses to cavity-creating mutations in hydrophobic cores: observation of a buried water molecule and the hydrophilic nature of such hydrophobic cavities. Biochemistry 35:4298–4305.
21. Baase WA, Liu L, Tronrud DE, Matthews BW (2010) Lessons from the lysozyme of phage T4. Protein Sci 19: 631–641.
22. Richards FM (1977) Areas, volumes, packing and protein structure. Annu Rev Biophys Bioeng 6:151–176.
23. Lim WA, Hodel A, Sauer RT, Richards FM (1994) The crystal structure of a mutant protein with altered but improved hydrophobic core packing. Proc Natl Acad Sci USA 91:423–427.
24. Ellerby LM, Escobar WA, Fink AL, Mitchinson C, Wells JA (1990) The role of lysine-234 in beta-lactamase catalysis probed by site-directed mutagenesis. Biochemistry 29:5797–5806.
25. Matagne A, Misselyn-Bauduin AM, Joris B, Erpicum T, Granier B, Frere JM (1990) The diversity and catalytic properties of class A β-lactamases. Biochem J 265:131–146.
26. Matagne A, Misselyn-Bauduin AM, Joris B, Erpicum T, Granier B, Frere JM (1990) The diversity of the catalytic properties of class A beta-lactamases. Biochem J 265:131–146.
27. Matagne A, Frere JM (1995) Contribution of mutant analysis to the understanding of enzyme catalysis: the case of class A beta-lactamases. Biochim Biophys Acta 1246:109–127.
28. Herzberg O, Moult J (1987) Bacterial resistance to beta-lactam antibiotics: crystal structure of beta-lactamase from *Staphylococcus aureus* PC1 at 2.5 A resolution. Science 236:694–701.
29. Myers JK, Pace CN, Scholtz JM (1995) Denaturant m values and heat capacity changes: relation to changes in accessible surface areas of protein unfolding. Protein Sci 4:2138–2148.
30. Serrano L, Kellis JT, Cann P, Matouschek A, Fersht AR (1992) The folding of an enzyme. II. Substructure of barnase. J Mol Biol 224:783–804.
31. Matthews BW (1993) Structural and genetic analysis of protein stability. Annu Rev Biochem 62:139–160.
32. Pace CN, Fu H, Fryar KL, Landua J, Trevino SR, Shirley BA, Hendricks MM, Iimura S, Gajiwala K, Scholtz JM, Grimsley GR (2011) Contribution of hydrophobic interactions to protein stability. J Mol Biol 408:514–528.
33. Frauenfelder H, Hartmann H, Karplus M, Kuntz ID, Jr, Kuriyan J, Parak F, Petsko GA, Ringe D, Tilton RF, Jr, Connolly ML, Max L (1987) Thermal expansion of a protein. Biochemistry 26:254–261.
34. Tilton RF, Jr, Dewan JC, Petsko GA (1992) Effects of temperature on protein structure and dynamics: X-ray crystallographic studies of the protein ribonuclease-A at nine different temperatures from 98 to 320 K. Biochemistry 31:2469–2481.
35. Juers DH, Matthews BW (2001) Reversible lattice repacking illustrates the temperature dependence of macromolecular interactions. J Mol Biol 311:851–862.
36. Rader SD, Agard DA (1997) Conformational substates in enzyme mechanism: the 120 K structure of alpha-lytic protease at 1.5 A resolution. Protein Sci 6:1375–1386.
37. Fraser JS, van den Bedem H, Samelson AJ, Lang PT, Holton JM, Echols N, Alber T (2011) Accessing protein

conformational ensembles using room temperature X-ray crystallography. Proc Natl Acad Sci USA 108: 16247–16252.
38. Urayama P, Phillips GNJ, Gruner SM (2002) Probing substates in sperm whale myoglobin using high-pressure crystallography. Structure 10:51–60.
39. Perilo CS, Pereira MT, Santoro MM, Nagem RA (2010) Structural binding evidence of the trypanocidal drugs berenil and pentacarinate active principles to serine protease model. Int J Biol Macromol 46:502–511.
40. Kellis JT, Jr, Nyberg K, Fersht AR (1989) Energetic of complementary side-chain packing in a protein hydrophobic core. Biochemistry 28:4914–4922.
41. Shortle D, Stites WE, Meeker AK (1990) Contributions of the large hydrophobic amino acids to the stability of staphylococcal nuclease. Biochemistry 29:8033–8041.
42. Varadarajan R, Richards FM (1992) Crystallographic structures of ribonuclease S variants with nonpolar substitution at position 13: packing and cavities. Biochemistry 31:12315–12327.
43. Takano K, Ogasahara K, Kaneda H, Yamagata Y, Fujii S, Kanaya E, Kikuchi M, Oobatake M, Yutani K (1995) Contribution of hydrophobic residues to the stability of human lysozyme: calorimetric studies and X-ray structural analysis of the five isoleucine to valine mutants. J Mol Biol 254:62–76.
44. Takano K, Yamagata Y, Fujii S, Yutani K (1997) Contribution of the hydrophobic effect to the stability of human lysozyme: calorimetric studies and X-ray structural analyses of the nine valine to alanine mutants. Biochemistry 36:688–698.
45. Xu J, Baase WA, Baldwin E, Matthews BW (1998) The response of T4 lysozyme to large-to-small substitutions within the core and its relation to the hydrophobic effect. Protein Sci 7:158–177.
46. Machicado C, Bueno M, Sancho J (2002) Predicting the structure of protein cavities created by mutation. Protein Eng 15:669–675.
47. DePristo MA, Weinreich DM, Hartl DL (2005) Missense meanderings in sequence space: a biophysical view of protein evolution. Nat Rev Genet 6:678–687.
48. Jansson JAT (1965) A direct spectrophotometric assay for penicillin ß-lactamase (penicillinase). Biochim Biophys Acta 99:171–172.
49. Humprey W, Dalke A, Schulten K (1996) VMD-Visual Molecular dynamics. J Mol Graphics 14:33–38.
50. Ambler RP, Coulson FW, Frere JM, Ghuysen JM, Joris B, Forsman M, Tiraby G, Waley SG (1991) A standard numbering scheme for the Class A β-lactamases. Biochem J 276:269–262.
51. Dundas J, Ouyang Z, Tseng J, Binkowski A, Turpaz Y, Liang J (2006) CASTp: computed atlas of surface topography of proteins with structural and topographical mapping of functionally annotated residues. Nucleic Acids Res 34:W116–W118.
52. Trapani S, Navaza J (2008) AMoRe: classical and modern. Acta Crystallogr D64:11–16.
53. Murshudov GN, Vagin AA, Dodson EJ (1997) Refinement of macromolecular structures by the maximum-likelihood method. Acta Crystallogr D 53:240–255.
54. Emsley P, Cowtan K (2004) Coot: model-building tools for molecular graphics. Acta Crystallogr D 60: 2126–2132.
55. Fersht AR (1999) Structure and mechanism in protein science: a guide to enzyme catalysis and protein folding. New York: Freeman.